Research Journal of Applied Sciences, Engineering and Technology 3(7): 602-611, 2011
ISSN: 2040-7467

Received: April 01, 2011 Accepted: May 18, 2011 Published: July 25, 2011

Magnetic Field Effect on the Electrical Parameters of a Polycrystalline Silicon Solar Cell

[1]A. Dieng, [1]N. Thiam, [1]A. Thiam, [2]A.S. Maiga and [1]G. Sissoko
[1]Laboratory of Semiconductors and Solar Energy, Physics Department, Faculty of Science and Technology, University Cheikh Anta Diop, Dakar, Senegal
[2]Applied Physics Department, UFR-SAT, University Gaston BERGER, St-Louis, Senegal

Abstract: In this study, we present a theoretical 3D study of a polycrystalline silicon solar cell in frequency modulation under polychromatic illumination and applied magnetic field. The influence of the applied magnetic field on the diode current density Jd, the both electric power-photovoltage and photocurrent-photovoltage characteristics are discussed. Nyquist diagram permitted to determine the electrical parameters such as series resistance Rs and parallel equivalent resistance Rp of a polycrystalline silicon solar cell. Bode diagram is then used to calculate the cut-off frequency, the capacitance C and inductance L. It has been shown that, under magnetic field, the solar cell behavior is like a low-pass filter.

Key words: Electrical parameters, frequency modulation, magnetic field, polycrystalline silicon

INTRODUCTION

Significant improvement of the solar cells performance has been made by controlling electrical parameters like open circuit voltage, short circuit current, shunt and series resistances and electronic parameters such as recombination velocities. With the new generation of p^+nn^+ solar cells, efficiencies of 19.1 and 18.1% are achieved under standard conditions when the cell is illuminated by nn^+ high-low junction and when it is illuminated by p^+n junction, respectively (Moehlecke *et al*., 1994). Efficiencies of 20 and 22.2%, are also achieved considering $Cu(In,Ga)Se_2$ polycrystalline thin-film and one-sun monocrystalline rear-contacted solar cells, respectively (Dicker *et al*., 2002).

The control of electrical and electronic parameters depends on their optimization in characterization studies. By the way, a schematic representation of the solar cell in its equivalent circuit (Chenvidhya *et al*., 2003) depending on operating conditions (steady state, transient and frequency modulation) can be used to extract some electrical parameters like series resistance, shunt resistance and space charge region capacitance.

Previous studies (Mbodji *et al*., 2009; Zouma *et al*., 2009) show that in transient state, the photocurrent, the photovoltage and the shunt resistance decrease while the series resistance increases with magnetic field and the internal quantum efficiency of the cell lessen.

In this study, we shall firstly solve the continuity equation with a 3D approach taking into account the grain size, the grain boundary recombination velocity and magnetic field in order to describe more accurately the dependencies between parameters. Secondly, the impedance spectroscopy method (Chenvidhya *et al*., 2003; Kumar *et al*., 2001; Steckl and Sheu, 1980) is used to determine electrical parameters such as series resistance, parallel resistance, equivalent capacitance and inductance for various magnetic field based on the electrical equivalent circuit of the solar cell in frequency modulation under polychromatic illumination (Pannalal, 1973-1974; Honma and Munakata, 1987).

Theory: This study is based on the following modelling of the polycrystalline silicon grain (Fig. 1):

- The grains have square cross section and their electrical properties are homogeneous; we can then use the cartesian coordinates
- The illumination is uniform so that the generation rate depend only on the depth in the base z
- The grain boundaries are perpendicular to the junction and their recombination velocities independent of generation rate under an illumination AM1.5. So the boundary conditions are linear
- The contribution of the emitter and space charge region is neglected, so this analysis is only developed in the base region

Corresponding Author: A. Dieng, Laboratory of Semiconductors and Solar Energy, Physics Department, Faculty of Science and Technology, University Cheikh Anta Diop, Dakar, Senegal

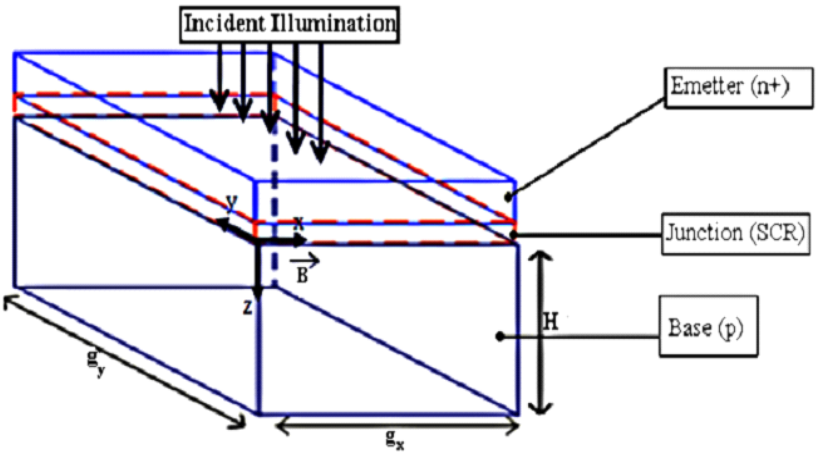

Fig. 1: Three-dimensional model of the polycrystalline silicon grain

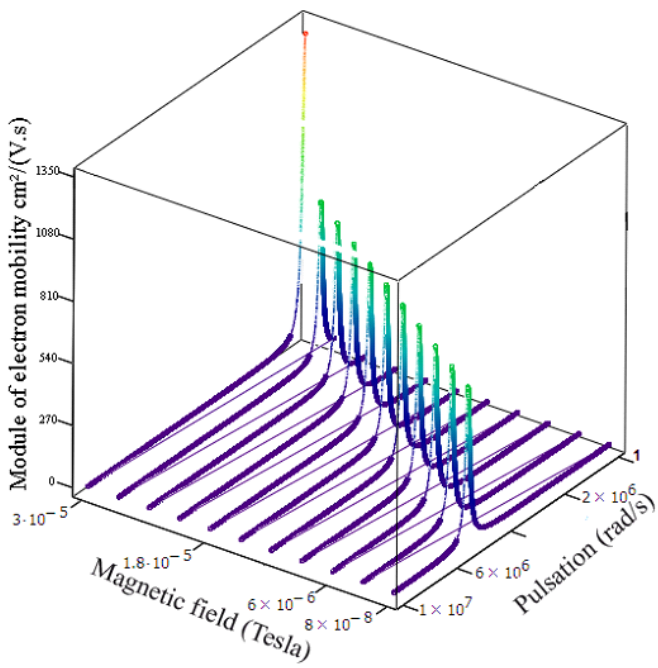

Fig. 2: Module of the mobility versus angular frequency for different magnetic field values

The continuity equation for the excess minority carrier density d(x,y,z,t) photogenerated in the base is:

$$D_n^* \cdot \left[\frac{\partial^2 \delta(x,y,z,t)}{\partial x^2} + \frac{\partial^2 \delta(x,y,z,t)}{\partial y^2} + \frac{\partial^2 \delta(x,y,z,t)}{\partial z^2} \right] \frac{\delta(x,y,z,t)}{\tau} + G(z,t) = 0 \qquad (1)$$

D_n^* and τ are respectively excess minority carrier diffusion constant and lifetime.

G(z,t) is a position dependent carrier generation rate in the base and can be written as (Furlan and Amon, 1985):

$$G(z,t) = G(z).e^{-iwt} \tag{2}$$

$$G(z) = \sum_{i=1}^{3} a_i.e^{-b_i Z} \tag{3}$$

Parameters a_i and b_i are coefficients deduced from modelling of the generation rate considered for overall the solar radiation spectrum when AM1.5 (Mohammad, 1987).

Electron's mobility: The electron's mobility (Seeger, 1973) in frequency modulation under magnetic field is given by:

$$\mu_n^* = \frac{\left[1+\left(\omega_p^2+\omega^2\right).\tau^2\right].\mu}{\left[1+\left(\omega_p^2+\omega^2\right).\tau^2\right]^2+4.\omega^2.\tau^2} + \frac{i.\omega.\tau.\left[\left(\omega_p^2-\omega^2\right).\tau^2-1\right].\mu}{\left[1+\left(\omega_p^2-\omega^2\right).\tau^2\right]^2+4.\omega^2.\tau^2} \tag{4}$$

A plot of electron's mobility versus angular frequency and magnetic field is presented on Fig. 2:

The module of the mobility (Fig. 2) decrease with the modulation frequency for various values of the magnetic field; we note the existence of peaks of resonance for magnetic field intensities higher than 10^{-7} Tesla.

We distinguish two zones for very weak magnetic fields:

- A first zone [1 rad/s; 10^4 rad/s] where the mobility remain practically constant (quasi-static mode)
- A second zone [10^4 rad/s; 10^7 rad/s] where the mobility decrease in a notable way (strong dependence on the angular frequency)

The application of a magnetic field, reveals a third zone where we obtain a resonance peak. This resonance phenomenon is obtained when the modulation frequency is equal to the cyclotron frequency.

The magnetic field applied to the photovoltaic cell tends to slow down the electrons coming from the base towards the junction by deviating them from their trajectory. Therefore we have a reduction of the effective mobility of the photogenerated carriers in the semiconductor.

Consequently, to make the study in frequency modulation, it is necessary to choose correct defined values of the magnetic field for the optimal answer of the photovoltaic cell.

Einstein-Smoluchowski relation gives (Sze and Kwok, 2007):

$$\frac{D_n^*}{\mu_n^*} = \frac{K.T}{e} \tag{5}$$

In frequency modulation and under magnetic field the expression of the diffusion constant is then given by the following relation:

$$D_n^* = \frac{\left[1+\left(\omega_p^2+\omega^2\right).\tau^2\right].D}{\left[1+\left(\omega_p^2-\omega^2\right).\tau^2\right]^2+4.\omega^2.\tau^2} + \frac{i.\omega.\tau.\left[\left(\omega_p^2-\omega^2\right).\tau^2-1\right].D}{\left[1+\left(\omega_p^2-\omega^2\right).\tau^2\right]^2+4.\omega^2.\tau^2} \tag{6}$$

$\omega_p = \frac{e^{*B}}{m^*}$ is the cyclotron frequency (Kittel, 1996; Cardona, 1969) (frequency of the electron on its orbit in the presence of a magnetic field).

B is the applied magnetic field and m* is electron effective mass.

Excess minority carrier density: A general solution of the continuity equation can be expressed as:

$$\delta(x,y,z,t) = \sum_k \sum_j Z_{kj} \cos(C_k.x) \cos(C_j.y) e^{-i\omega t} \tag{7}$$

where c_k and c_j are obtained from the following boundary conditions:

- In the x direction, at $x = \pm\frac{g_x}{2}$

$$D_n^* \left[\frac{\partial\delta(x,y,z)}{\partial_x}\right]_{x=\pm\frac{g_x}{2}} = \mp Sgb.\delta\left(\pm\frac{g_x}{2},y,z\right) \tag{8}$$

- In the y direction, at $y = \pm \frac{g_y}{2}$

$$D_n^* \left[\frac{\partial \delta(x,y,z)}{\partial y} \right]_{y=\pm\frac{g_y}{2}} = \mp Sgb.\delta\left(x, \pm \frac{g_y}{2}, z \right) \quad (9)$$

Equation (8) and (9) define a grain boundary recombination velocity Sgb that traduces how excess carriers flow through grain boundaries, g_x and g_y are the grain sizes on the x and y direction, respectively.

Replacing d(x,y,z) by its expression into the above two boundary conditions and rearranging the different terms, we obtain the following transcendental equations:

$$C_k \tan\left(C_k \frac{g_x}{2} \right) = \frac{Sgb}{D_n^*} \quad (10)$$

and

$$C_j \tan\left(C_j \frac{g_y}{2} \right) = \frac{Sgb}{D_n^*} \quad (11)$$

C_k and C_j are the eigen values of these transcendental equations solved numerically. Replacing d(x,y,z) in the continuity equation and using the fact that the cosine functions are orthogonal we obtain a differential equation leading to the expression of $Z_{kj}(z)$:

$$Z_{kj}(z) = A_{kj} \cosh\left(\frac{z}{L_{kj}} \right) + B_{kj} \sinh\left(\frac{z}{L_{kj}} \right) + \sum_{i=1}^{3} C_i e^{-b_i z} \quad (12)$$

with

$$C_i = \frac{n\left(L_{kj}\right)^2 . a_i}{D_{kj}\left(\left(L_{kj}\right)^2 . b_i^2 - 1\right)} \quad (13)$$

where;

$$D_{kj} = \frac{D\left[C_k . g_x + \sin\left(C_k . g_x\right)\right]\left[C_{kj} . g_y + \sin\left(C_j . g_y\right)\right]}{16.\sin\left(C_k . \frac{g_x}{2}\right)\sin\left(C_j \frac{g_y}{2}\right)} \quad (14)$$

and

$$L_{kj} = \sqrt{\frac{1}{\frac{1}{L^2} + C_k^2 + C_j^2}} \quad (15)$$

Constants A_{kj} and B_{kj} are calculated by mean of the boundary conditions (Dugas, 1994; Joshi and Bhatt, 1990):

- At the n^+p interface (z = 0):

$$D_n^* \left[\frac{\partial \delta(x,y,z)}{\partial_z} \right]_{z=H} = -Sb.\delta(x,y,0) \quad (16)$$

- At the back surface (z = H):

$$D_n^* \left[\frac{\partial \delta(x,y,z)}{\partial_z} \right]_{z=H} = -Sb.\delta(x,y,H) \quad (17)$$

Sf is the sum of two contributions: Sf_0 which is the intrinsic junction recombination velocity induced by the shunt resistance and Sf_j which traduces the current flow imposed by an external load and defines the operating point of the cell:

$$Sf = Sf_0 + Sf_j$$

(Sissoko *et al*., 1992; Diallo *et al*., 2008; Madougou *et al*., 2007). Sb is the effective back surface recombination velocity.

The photocurrent is given by the following expression:

$$J_{ph} = \frac{q.D_n^*}{gx.gy} \int_{\frac{g_x}{2}}^{+\frac{g_x}{2}} \int_{\frac{g_y}{2}}^{\frac{g_y}{2}} \left[\frac{\partial \delta(x,y,z)}{\partial_z} \right]_{z=0} dxdy \quad (18)$$

The diode current is a leakage current which characterizes the losses of photogenerated charge carriers and depends on the intrinsic junction recombination velocity (Dugas, 1994).

$$J_d = qSf_0 \int_{-\frac{g_x}{2}}^{+\frac{g_x}{2}} \int_{-\frac{g_y}{2}}^{+\frac{g_y}{2}} \left[\frac{\partial \delta(x,y,z)}{\partial_z} \right]_{z=0} dxdy \qquad (19)$$

The photovoltage is given by the expression below (Cardona, 1969):

$$v = v_T In\left[1 + \frac{N_b}{n_i^2} \int_{-\frac{g_x}{2}}^{+\frac{g_x}{2}} \int_{-\frac{g_y}{2}}^{+\frac{g_y}{2}} \delta(x,y,0) dxdy \right] \qquad (20)$$

The electric power is an essential parameter for the solar cell. It indicates the capacity of the solar cell to provide electricity to the external load; the electric output (Mishra and Singh, 2008) provided by the solar cell for a polychromatic illumination is expressed as follows:

$$P = V \cdot J \qquad (21)$$

with

$$J = J_{ph} - J_d \qquad (22)$$

The conversion efficiency is the ratio between the maximum electric output provided by the solar cell and the power of the incident light received by the photovoltaic cell (100 mW/cm^2 in this study).

$$\eta = \frac{pm}{pinc} \qquad (23)$$

The dynamic impedance of the solar cell is given by the equation below (Barsoukov and Macdonald, 2005):

$$Z_{ph} = \frac{V_{ph}}{V_{ph}} \qquad (24)$$

RESULTS AND DISCUSSION

Diode current: Application of the magnetic field induces a resonance phenomenon on the diffusion constant and diffusion length.

We present the diode current of the photovoltaic cell versus recombination velocity (semi- logarithmic scale) for various values of the magnetic field (Fig. 3):

We distinguish two zones:

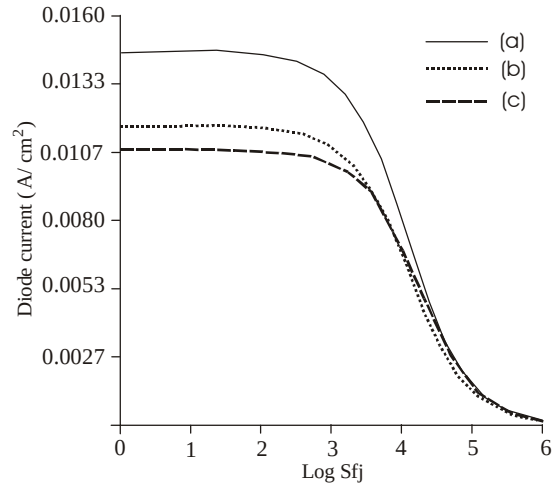

Fig. 3: Diode current versus logarithm of Sf_j
(a) B = 1×10^{-8} T , ωp = 20000 rad/s
(b) B = 1.5×10^{-5}T, $\omega_p = 2.64\times10^6$ rad/s
(c) B = 3.0×10^{-5}T, $\omega_p = 5.28\times10^6$ rad/s

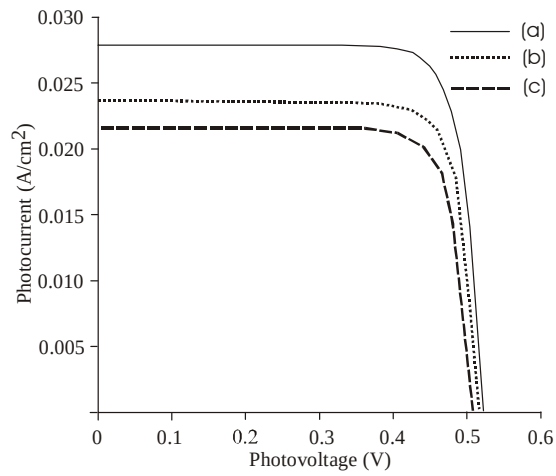

Fig. 4: I-V curves
(a) B = 1×10^{-8} T, ω_p = 20000 rad/s
(b) B = 1.5×10^{-5} T, $\omega_p = 2.64\times10^6$ rad/s
(c) B = 3.0×10^{-5} T , $\omega_p = 5.28\times10^6$ rad/s

- A first zone [From Sf_j = 1 cm/s to $Sf_j = 10^3$ cm/s] where the diode current remains practically constant
- A second zone [From $Sf_j = 10^3$ cm/s to $Sf_j = 10^6$ cm/s] where the diode current decreases in a notable way

If $Sf_j \geq 10^6$ cm/s, there is practically no current.

We note that the diode current decreases with the increase of the modulation frequency and the magnetic field at the resonance.

I-V Characteristics: The photocurrent-photovoltage curve of the solar cell for various values of the magnetic field is given below (Fig. 4).

Under frequency modulation, for a given value of the magnetic field, we place ourselves at electron cyclotron resonance in order to optimize the answer of the photovoltaic cell.

Thus the I-V curve of the photovoltaic cell under magnetic field comprises two zones:

- A first zone for [0 volt - 0.40 volt], where the photocurrent remains practically constant
- A second zone for [0.40 volt - 0.53 volt] where the photocurrent decrease quickly before being cancelled at the open circuit

Let us note that the short-circuit photocurrent and the open circuit photo voltage decrease with increasing magnetic field. This undoubtedly will involve a reduction in the maximum power of the solar cell.

P-V Characteristics: The power of the photovoltaic cell for various magnetic field values is presented on (Fig. 5).

The solar cell's electric power varies linearly with the phototension until the maximum power and then decreases rapidly. The increase of the magnetic field lead to a decrease in the maximum power of the cell (curves a®c) as previously noted.

Photovoltaic conversion efficiency: We present on (Fig. 6) the conversion efficiency versus boundary recombination velocity and magnetic field.

We note that the effects of the magnetic field and grain boundary recombination velocity on the photovoltaic cell in frequency modulation is a reduction of the conversion efficiency, due to the reduction of the diffusion length with the magnetic field and also to the carriers lost at the grain boundary with increasing grain boundary recombination velocity.

Solar cell impedance:

Bode diagram: Bode diagram (Pannalal, 1973-1974) is used to access to the cut-off frequency. We plot respectively the impedance module (ïZï) and impedance phase versus modulation frequency in a semi-logarithmic scale.

Module: Impedance module versus angular frequency for various magnetic field is plotted on (Fig. 7) in a semi logarithmic scale.

The intersection of the prolongations of each of the two linear parts of the curve enables us to obtain the cut-off frequency ω_c.

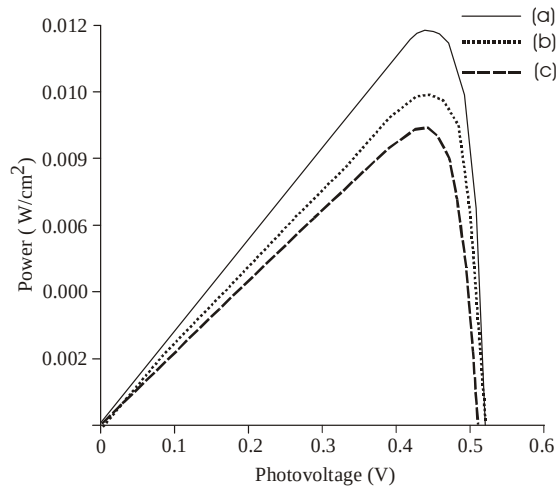

Fig. 5: P-V curves
(a) $B = 1\times10^{-8}$ T, $\omega_p = 20000$ rad/s
(b) $B = 1.5\times10^{-5}$ T, $\omega_p = 2.64\times10^{6}$ rad/s
(c) $B = 3.0\times10^{-5}$ T, $\omega_p = 5.28\times10^{6}$ rad/s

Table 1: Cut-off frequency ω_c according to the magnetic field

B (Tesla)	10^{-8}	1.5×10^{-5}	3.0×10^{-5}
Cut-off frequency	ω_{c1}	ω_{c2}	ω_{c3}
w_c(rad/s)	141600	79620	48530

The Table 1 gives the values of the cut-off frequency ω_c according to the magnetic field. When the magnetic field is weak (in the order 10^{-8} Tesla), Figure 8a, for the angular frequencies included in interval $0 < \omega < \omega_{c1}$ the module of the impedance is independent on the frequency. For the values of the pulsation such as $\omega > \omega_{c1}$ the module of the impedance increases with the angular frequency.

For an intense magnetic field (Fig. 8b and c), for angular frequencies in the range $0 < \omega < \omega_{c2,c3}$, the module of the impedance is independent of the frequency. For angular frequency such as $\omega > \omega_{c2,c3}$ the module of the impedance decrease with the angular frequency. When a magnetic field is applied, the photovoltaic cell behaves like a low-pass filter.

A low-pass filter in general enables us to get rid of the parasitic phenomena (smoothing). Within the framework of our work the intrinsic parasitic phenomena with the photovoltaic cell are the recombination with the junction and the back face. Our system (photovoltaic cell) can be regarded as a second-order low-pass filter for the values of the considerable magnetic field.

Phase: The phase diagram of the impedance for various magnetic field values is given on Fig. 8.

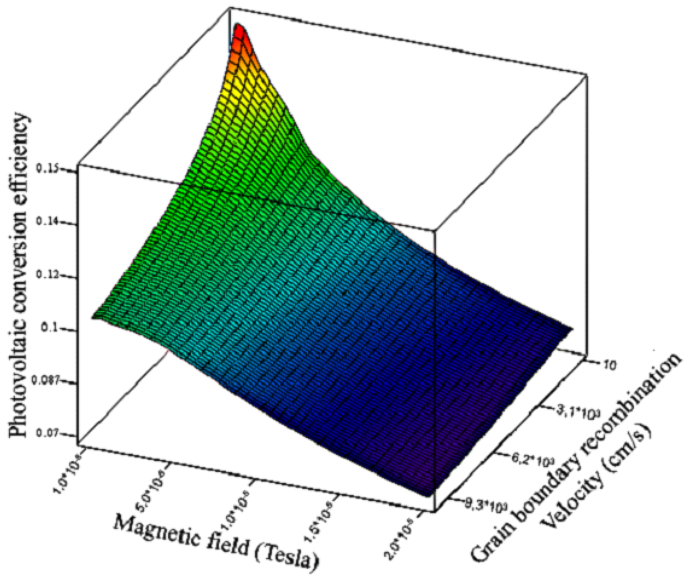

Fig. 6: Conversion efficiency profile versus grain boundary for various magnetic field values ($g_x = g_y = 120$ µm; $\omega = 1$ rad/s)

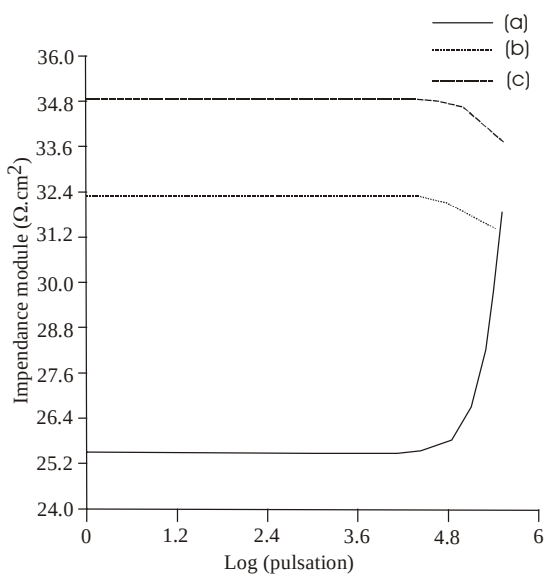

Fig. 7: Impedance amplitude versus angular frequency logarithmic scale ($g_x = g_y = 80$ µm; Sgb = 50 cm/s and Sf = 1000 cm/s)
(a) $B = 10^{-8}$ Tesla; (b) $B = 1.5\times10^{-5}$ T et; (c) $B = 3.0\times10^{-5}$T

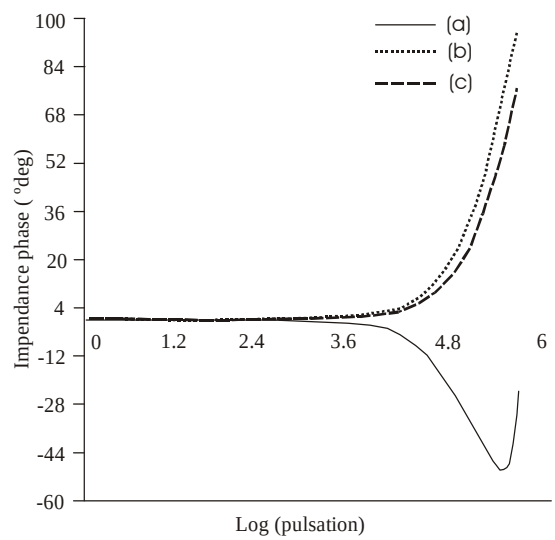

Fig. 8: Impedance phase versus angular frequency logarithmic scale ($g_x = g_y = 80$ µm; Sgb = 50 cm/s et Sf = 1000 cm/s)
(a) $B = 10^{-8}$ Tesla
(b) $B = 15.10^{-6}$ T
(c) $B = 3.0\times10^{-5}$ T

Fig. 8 show that for a weak magnetic field (curve a):

- For angular frequencies in the interval $0 < \omega < \omega_1$, the phase of the impedance is independent of the frequency: that is we are still in a quasi-steady state.
- For angular frequencies in the interval $\omega_1 < \omega < \omega_2$, the phase of the impedance decrease quickly with the angular frequency: The modulation frequency begins here.

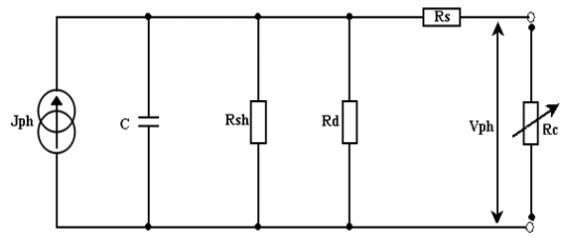

Fig. 9: Equivalent circuit of the solar cell ($g_x = g_y = 80$ µm; Sgb = 50 cm/s and Sf =1000 cm/s)

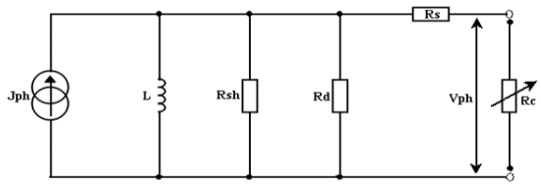

Fig. 10: Equivalent circuit of the solar cell

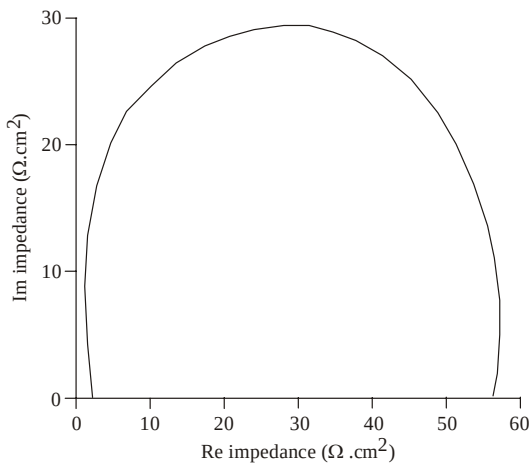

Fig.11a: Im(Z) versus Re(Z) ($g_x = g_y = 80$ µm; Sgb = 50 cm/s and Sf =1000 cm/s) B = 10^{-8} Tesla

- For the values of the pulsation such as $\omega < \omega_2$ the phase of the impedance increases with the angular frequency.

For a most important magnetic field (curve b and curve c), when the angular frequencies are in the interval $0 < \omega < \omega_1$, the phase of the impedance is independent of the frequency.

For the values of the pulsation such as $\omega > \omega_1$ the phase of the impedance increases with the pulsation.

The Bode diagram of the phase for various values of the applied magnetic field enables us to validate the

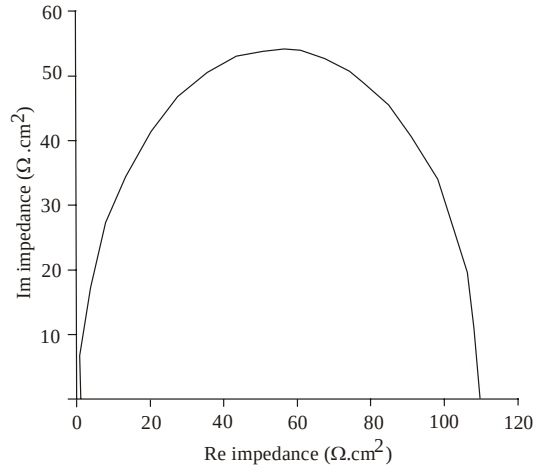

Fig. 11b: Im(Z) versus Re(Z) ($g_x = g_y = 80$ µm; Sgb = 50 cm/s and Sf = 1000 cm/s) B = $1.5.0\times10^{-5}$ T

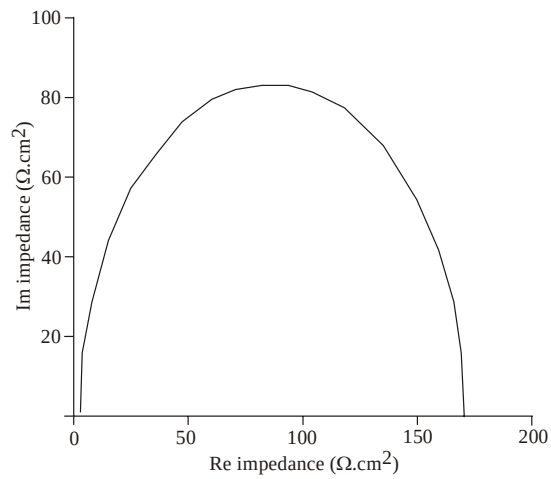

Fig.11c: Im(Z) versus Re(Z) ($g_x = g_y = 80$ µm; Sgb = 50 cm/s and Sf =1000 cm/s) B 3.0×10^{-5} T

model where the capacitive effects prevail for a weak magnetic field (of the order 10^{-8} Tesla) and the inductive model where the inductive effects prevail for a considerable magnetic field.

Equivalent circuit of a solar cell:
We propose two electric models:

- **A first model that comprises a series resistance, a dynamic resistance, a shunt resistance and a capacitance:** In this model, the capacitive effects of space charge region can be put forward by replacing the diode by an equivalent capacitance (capacitance resulting from diffusion, recombination centers and transition capacitance) and a dynamic resistance

which are in parallel. In this first model the capacitive effects prevail.

The electric model in frequency modulation is represented in Fig. 9 (Zouma *et al*., 2009; Anil Kumar *et al*., 2001).

- **The second model comprises a series resistance, a dynamic resistance and a shunt resistance and an inductance:** In the second model, the diode is modeled by an inductance and a resistance in parallel. In this model the inductive effects are predominant.

The electric model of the photovoltaic cell in frequency modulation is represented in Fig. 10 where, the inductive effect is taken into account (Kleveland *et al*., 1999; Kumar, 2000).

- C is the sum of C_D , C_T and $C_R C_D$ is the diffusion capacitance; it is due to the diffusion of the minority carriers excess in the cell
- C_T is the transition capacitance; it is due to the variation of the density in the space charge region (SCR).
- C_R is a capacitance due to the recombination centers in the space charge
- R_{sh} models leakage currents existing at the edge of the structure and the defects in the vicinity of the space charge region (dislocation, grain boundary).
- R_D is the dynamic resistance of the intrinsic diode in the solar cell
- R_s is the dynamic resistance of the intrinsic diode in the solar cell and represents the resistive losses in the cell (material resistivity, metallization).
- L is and inductance due to the fact that material and metallization resistivity's are dependent of the modulation frequency.

NYQUIST diagram: The NYQUIST diagram of solar cell impedance Z (Honma and Munakata, 1987; Pereira *et al*., 2006) is plotted below for various magnetic field values (Fig. 11a, b and c).

It is observed on these figures that when the intensity of the applied magnetic field increases, the series and parallel resistances increase also. Consequently, the action of the magnetic field leads to an increase of the voltage drop in the cell and a slight increase of the output current.

The Table 2 gives the values of series and parallel resistances for various magnetic field values. The associated capacitance and inductance are then deduced and presented in the Table 3.

Table 2: Series and parallel resistance for various magnetic field intensities

B (Tesla)	Rs (Ω.cm^2)	Rp (Ω.cm^2)
10^{-8}	1.3	56.1
1.5×10^{-5}	1.9	108.4
3.0×10^{-5}	2.4	167.9

Table 3: Capacitance/ inductance for various magnetic field intensities.

B (Tesla)	10^{-8}	1.5×10^{-5}	3.0×10^{-5}
C (μF.cm^2)	7.45×10^{-1}		
L (μH.cm^2)		7.28×10^{-1}	7.75×10^{-1}

CONCLUSION

Based on an AC- equivalent circuit of the solar cell an expression of its impedance has been established, composed in two parts: imaginary and real parts that vary with modulation frequency and applied magnetic field. From both Nyquist and Bode diagrams, solar cell electrical parameters has been determined and the influence of the applied magnetic field is shown for a given grain size and grain boundary recombination velocity: series resistance, parallel resistance and space charge region capacitance increase with increasing magnetic field because of the solar cell magnetoresistance. The dependence of the phase of the dynamic impedance shows that for high magnetic values, the solar cell becomes more and more inductive (no capacitive part) so that the AC- equivalent circuit of the cell must be modified. The conversion efficiency is also very dependent on the applied magnetic field.

ACKNOWLEDGMENT

The authors would like to thank Mr. Assani Dahouenon (GIZ-Senegal/PERACOD) and the team of "Renewable Energy International Research Group".

REFERENCES

Anil Kumar, R., M.S. Suresh and J. Nagaraju, 2001. Measurement of AC parameters of gallium arsenide (GaAs/Ge) solar cell by impedance spectroscopy. IEEE Trans. Electron Dev., 48(9): 2177-2179.

Anil Kumar, R., 2004. Studies on solar cell AC parameters. M.Sc. Thesis, Indian Institute of Science.

Barsoukov, E. and J.R. Macdonald, 2005. Impedance Spectroscopy: Theory, Experiment and Applications. 2nd Edn., 0 John Wiley and Sons.

Cardona, M., 1969. Modulation spectroscopy. Solid State Phys., Suppl, 11.

Chenvidhya, D., K. Kirtikara and C. Jivacate, 2003. A new characterization method for solar cell dynamic impedance. Solar Energ. Mat. Sol. C., 80(4): 459-464.

Diallo, H.L.,A. Wereme,A.S. Maïga and G. Sissoko, 2008. New approach of both junction and back surface recombination velocities in a 3D modelling study of a polycrystalline silicon solar cell. Eur. Phys. J. Appl. Phys., 42(3): 203-211.

Dicker, J., J.O. Schumacher, W. Wart and W. Glunz, 2002. Analysis of one-sun monocrystalline rear-contacted silicon solar cells with efficiencies of 22.1%. J. Appl. Phys., 91(7): 44335-4344.

Dugas, J., 1994. 3D modelling of a reverse cell made with improved multicrystalline silicon wafers. Solar Energ. Mat. Solar Cells, 32: 71-88.

Furlan, J. and S. Amon, 1985. Approximation of the carrier generation rate in illuminated silicon. Solid State Electr., 28(12): 1241-1243.

Honma N. and C. Munakata, 1987. Sample Thickness Dependence of Minority Carrier Lifetimes Measured Using an ac Photovoltaic Method. Japanese J. Appl. Phys., 26(12): 2033-2036.

Joshi, D.P. and D.P. Bhatt, 1990. Theory of grain boundary recombination and carrier transport in polycrystalline silicon under optical illumination. IEEE Trans. Electron Dev., 37(1): 237.

Kleveland, B., X. Qi, L. Madden, R.W. Dutton and S.S. Wong, 1999. Line inductance extraction and modeling in a real chip with power grid. Technical Digest of IEEE International Electron Devices Meeting (IEDM), pp: 901-904.

Kittel, C., 1996. Introduction to Solid State Physics. 7th Edn., John Wiley and Sons, New York.

Madougou, S., F. Made, M.S. Boukary and G. Sissoko, 2007. I-V characteristics for bifacial silicon solar cell studied under a magnetic field. Adv. Mat. Res., 18-19: 303-312.

Mbodji, S., A.S. Maïga, M. Dieng, A. Wereme and G. Sissoko, 2009. Removal Charge technique applied to a bifacial solar cell under constant magnetic field. Global J. Pure Appl. Sci., 15(1): 125-132.

Mishra, U K. and J. Singh, 2008. Semiconductor Device Physics and Design. Springer, pp: 189.

Moehlecke, A., I. Zanesco and A. Luque, 1994. Practical high efficiency bifacial solar cells. IEEE Phot. Spec. Conf., 2: 1663-1666.

Mohammad, S.N., 1987. An alternative method for the performance analysis of silicon solar cells. J. Appl. Phys., 61(2): 767-772.

Pannalal, L.B., 1973-1974. Signals, Systems and Controls. Intext Educational Publisher, New York.

Pereira, L., L. Raniero, P. Barquinha, E. Fortunato and Martins, 2006. Impedance study of the electrical properties of poly-Si thin film transistors. J. Non-Cryst. Solids, 352(9-20): 1737-1740.

Seeger, K., 1973. Semiconductor physics. Springer-Verlag. ISBN: 0-387-81186-9) New York, pp: 269.

Sissoko, G., S. Sivoththanam, M. Rodot and P. Mialhe, 1992. Constant illumination-induced open circuit voltage decay (CIOCVD) method, as applied to high efficiency Si Solar cells for bulk and back surface characterization. 11th European Photovoltaic Solar Energy Conference and Exhibition, poster 1B, 12-16, pp: 352-354.

Steckl, A.J. and S.P. Sheu, 1980. The AC admittance of the p-n PbS-Si heterojunction. Solid State Electron., 23: 715-720.

Sze, S.M. and K. Ng Kwok, 2007. Physics of Semiconductors Devices. 3rd Edn., John Wiley and Sons.

Zouma, B., A.S. Maïga, M. Dieng, F. Zougmore and G. Sissoko, 2009. 3d Approach of spectral response for a bifacial silicon solar cell under a constant magnetic field. Global J. Pure Appl., 15(1): 117-124.